Available online at www.sciencedirect.com

SciVerse ScienceDirect

Ceramics International 39 (2013) 7657–7668

CERAMICS INTERNATIONAL

www.elsevier.com/locate/ceramint

Effect of metallic Si addition on polymerization degree of *in situ* foamed alkali-aluminosilicates

Valentina Medri[a,*], Elettra Papa[a], Jiri Dedecek[b], Hana Jirglova[b], Patricia Benito[c], Angelo Vaccari[c], Elena Landi[a]

[a]*National Research Council of Italy, Institute of Science and Technology for Ceramics (CNR-ISTEC), via Granarolo 64, 48018 Faenza, RA, Italy*

[b]*J. Heyrovsky Institute of Physical Chemistry ASCR, Dolejskova 2155/3, 18223 Prague 8, Czech Republic*

[c]*Dipartimento di Chimica Industriale "Toso Montanari", ALMA MATER STUDIORUM, Università di Bologna, Viale Risorgimento 4, 40136 Bologna, Italy*

Received 11 December 2012; received in revised form 22 February 2013; accepted 22 February 2013
Available online 25 March 2013

Abstract

Geopolymerization is an aqueous based process to produce synthetic alkali-aluminosilicates with porosity that can be tailored from the nano- to the ultra-macrometric range. In order to fulfill the requirements for many different applications and porous 3D networks (namely alkali-aluminosilicate foams) were prepared by inducing interconnected ultra-macro-porosity (up to the millimeter range) in the alkali-bonded matrices, exploiting the ability of silicon powder to generate H_2 in the aqueous medium. Being H_2 the product of a water-consuming process which competes with geopolymerization, the process parameters and the characteristics of the resulting foamed materials are strongly influenced by the amount of added silicon. Polymerization degree, accessibility of the geopolymer inner volume and the micro-ultra-macro-structure of the foams were determined and related to the process parameters of the contemporary geopolymerization and foaming.

Keywords: B. Porosity; Alkali-bonded ceramics; Geopolymerization; Foam; Silicon

1. Introduction

Porous ceramics have been extensively used because of their high specific surface area, permeability, sound absorption, thermal insulating and other properties [1]. Industrial uses include structural lightened parts, insulator panels, filters and membranes, radiant burners, gas or chemical sensors, support materials for catalysis or adsorbents.

For all the mentioned applications, it is absolutely necessary to control porosity, in terms of the following: pore size dimension and distribution; amount and pore structure (shape, morphology, orientation, and surface properties). For example, the required pore dimension for molecular sieves ranges from 1 Å to 1 nm; for sorbents from 1 Å to a few tenths of nanometers; for catalysts and supports from 1 nm to few tenth of microns; for filtering and purification systems from few nanometers to a few millimeters; and for dust collecting from few micrometers to few millimeters [1,2]. A porosity amount over 50% and up to 95% is required in view of a lightweight device [3] and thermal insulation [2]; porous ceramics with three-dimensionally interconnected and distributed open pores (3D structures) are useful as catalysts, catalyst supports, filters, and scaffolds, adsorbents, because of the high accessibility of pores [1,2,4].

Specific porous materials, such as zeolites, meso-porous silica, gels, ceramic membranes, ceramic foams, etc., are used to fulfill specific porosity requirements in view of specific applications [1,2].

Synthetic alkali-aluminosilicates, namely alkali-bonded ceramics or geopolymers [5,6], were produced by reacting an aluminosilicate powder with an aqueous alkali hydroxide and/or alkali silicate solution. They could be used to develop porous ceramic materials and components which cover the pore size range from a few tenths of nanometers to few millimeters and total porosity amount from 30% up to 90%. They are amorphous to semi-crystalline materials with three-dimensional aluminosilicate network, formed by condensation polymerization. The final microstructure of a fully

*Corresponding author. Tel.: +39 0546699751; fax: +39 054646381.
E-mail address: valentina.medri@istec.cnr.it (V. Medri).

0272-8842/$ - see front matter © 2013 Elsevier Ltd and Techna Group S.r.l. All rights reserved.
http://dx.doi.org/10.1016/j.ceramint.2013.02.104

reacted geopolymer matrix consists of nano-particulates ranging from 5 to 15 nm, separated by pores in the nanometric range [7,8]. On the atomic scale, geopolymer amorphous network is formed by SiO_4 and AlO_4 tetrahedra shearing oxygen corners. Recent results indicate that these tetrahedrons form in the network rings of various sizes analogous to those in zeolites. The formation of geopolymer network from Si–O–Al–O rings results, in analogy with zeolites, in ion exchange properties of geopolymer matrix [9,10]. Thus, geopolymers can be regarded as the amorphous counterpart or precursor of crystalline zeolites.

Chemical consolidation by geopolymerization and contemporary *in situ* inorganic foaming are suitable to produce ceramic foams with 3D porous architectures without using high temperature treatments (such as burnout of organics and sintering) that are indeed necessary for the production of ultramacroporous ceramics using conventional techniques [11].

In detail, *in situ* inorganic foaming can be obtained causing gas evolution in the geopolymer mixture [12–16]. The Pourbaix diagram of silicon indicates that in alkaline conditions hydrogen evolution is always favoured [17], following the reaction:

$$Si^0 + 4H_2O \rightarrow 2H_2\uparrow + Si(OH)_4, \quad \Delta H^0_{298K} = -314.0\ kJ/mol \tag{1}$$

In a previous study [8] optimal geopolymerization conditions were determined to develop porous 3D networks by inducing interconnected ultra-macro-porosity (up to the millimeter range) in selected alkali-aluminosilicate material, using low amount (≤0.03 wt%) of metallic silicon powder as a foaming agent. However, the solutions for specific application requirements must be tailored by a correct mixture and process design to optimize properties and possibly reduce costs. This work reports on several aspects of the intrinsic structures and properties of inorganic polymers, as well as on some of the extrinsic properties that may be conferred by an appropriate raw material selection, mixture and process design.

In particular, aim of this study is to check the effect of increasing Si^0 additions (≥0.03 wt%) on *in situ* foamed alkali-aluminosilicates to correlate the effect of heat release, occurring during the redox reaction (1), to the degree of polymerization (namely the conversion of aluminosilicate raw powder into geopolymer) and thus to the final micro- and macrostructure of the obtained foams. For this purpose, the developed alkali-aluminosilicate foams were fully characterized in term of microstructure, intrinsic and induced porosity size distribution, specific surface area, polymerization degree and ion exchange capacity.

2. Experimental procedure

2.1. Preparation of geopolymer foams

Metakaolin grade M1200S was purchased from AGS Minéraux, Clérac, France. For more details on powder characteristics see Refs. [10,18]. Potassium silicate solutions with molar ratios of SiO_2/K_2O=2 and H_2O/K_2O=13.5 and 23.0 were prepared by dissolving KOH pellets (purity > 98%, Merck, Darmstadt, Germany) into distilled water and adding fumed silica powder (99.8%, Sigma-Aldrich, Steinheim, Germany) under magnetic stirring. Metallic silicon powder (grade AX10, H.C. Stark, purity 99.995%, D50=4.50 μm) was used as a foaming agent.

Geopolymer slurries with Si/Al and K/Si atomic ratios, respectively, equal to 2.00 and 2.33 were prepared by mechanically mixing the metakaolin with the KOH/K_2SiO_3 aqueous solutions for 19 min at 100 r.p.m" for clarity, and correct if necessary. –>. Foams were prepared by adding from 0.03 to 2.60 wt% of Si powder into the geopolymer slurries. The Si/Al and K/Si nominal atomic ratios of the foam formulations were consequently higher than those of the starting geopolymeric slurries; values ranging from 2.01 to 2.36 for Si/Al and from 2.33 to 2.75 for K/Si were experimented.

Then mechanical mixing was performed for another minute after metallic silicon additions.

The slurries (20 ml) were cast in plastic cylindrical open molds with a diameter of 40 mm and maturated at room temperature (RT), 40 °C, 60 °C or 80 °C for 24 h. The foam expansion mainly occurred in the axial direction of the cylindrical mold. After curing,

Table 1
Si/Al and Si/K atomic ratios in alkali-aluminosilicate foams compositions, polymerization degree obtained from ^{27}Al MAS NMR and NH_4^+ exchange capacity, namely accessibility of the geopolymer inner volume.

Sample	Si/Al atomic ratio	Si/K atomic ratio	Polymerization degree (%)[a]	Accessibility (%)[b]
F13-0.38%Si-RT	2.05	2.39	56	25
F13-0.38%Si-80°C	2.05	2.39	48	23
F13-1.15%Si-RT	2.14	2.49	56	18
F13-1.15%Si-40°C	2.14	2.49	53	23
F13-1.15%Si-60 °C	2.14	2.49	39	16
F13-1.15%Si-80°C	2.14	2.49	51	15
F13-1.90%Si-RT	2.23	2.60	52	16
F13-1.90%Si-40 °C	2.23	2.60	42	11
F13-1.90%Si-60°C	2.23	2.60	30	17
F13-1.90%Si-80 °C	2.23	2.60	50	16
F13-0.04%Si-RT	2.01	2.33	97	27
F23-0.03%Si-RT	2.01	2.33	97	26

[a]The data errors for polymerization degree is ±5% and ±1% for polymerization degrees below and above 70%, respectively.
[b]The data error for accessibility of geopolymer network is ±5%.

foams were let at 80 °C for another 24 h to complete the setting process.

Foams prepared from potassium silicate solutions with molar ratios $H_2O:K_2O$=13.5 and 23.0 were named F13 and F23, respectively. Si wt% and the curing temperature were also reported in the labeling (see Table 1).

2.2. Characterization

Geopolymer slurries with H_2O/K_2O = 13.5 and 23.0 and without metallic silicon addition were characterized with a controlled-stress rotational rheometer (Bohlin C-VOR 120, Malvern, UK) equipped with parallel plate sensor with diameter 20 mm (PP20) and forcing the gap to 1 mm. Flow curves were determined by increasing the shear rate from 0 to 100 s^{-1} and then by decreasing from 100 to 0 s^{-1}.

The increase of the temperature in the geopolymer slurries related to metallic silicon addition was monitored by inserting a thermometer (range 0–100 °C with an accuracy of ± 0.5 °C) in the reaction mixtures at different times.

The morphological and microstructural features of foams were examined by SEM-EDS (SEM, Cambridge S360; EDS, INCA Energy 300, Oxford Instruments, Oxford, UK) samples were coated using a gold sputter coater.

The bulk density of the foams was determined by weight-to-volume ratio. The volume was geometrically measured using a calliper (accuracy ± 0.05 mm). The per cent values of total porosity of the foams were calculated according to the following equation:

$$\text{Total porosity}\ (\%) = [1-(\text{bulk density}/\text{true density})]\times 100 \quad (2)$$

where true density measured by Helium pycnometer (Multivolume pycnometer 1305 by Micrometrics) is 2.188 ± 0.002 g/

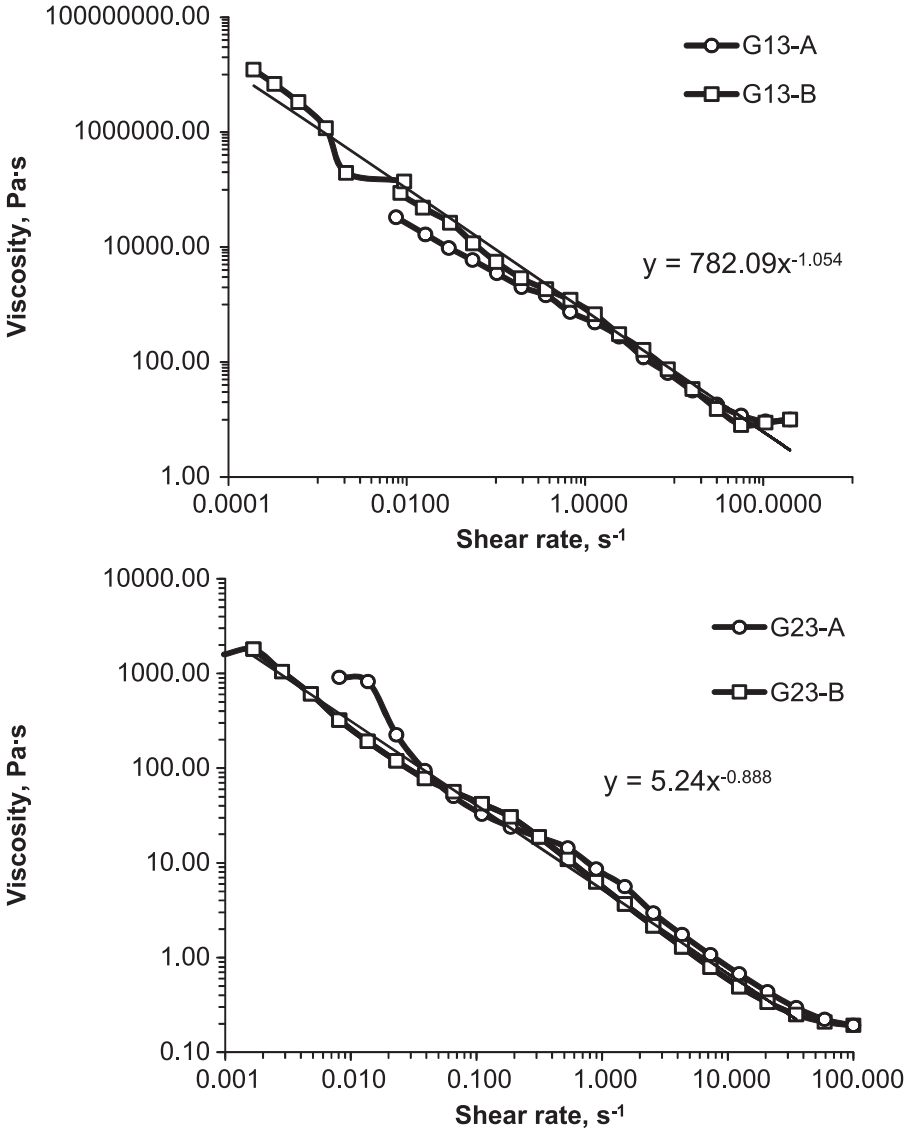

Fig. 1. Logarithmic plots of viscosity vs. shear rate of the geopolymer slurries with H_2O/K_2O = 13.5 and 23.0 and no metallic silicon addition. The data error is ± 5%. The fitting equations were calculated on the data recorded by decreasing the shear rate from 100 to 0 s^{-1}.

cm^3 and 2.246 ± 0.008 g/cm^3 for geopolymer matrices, respectively, in F13 and F23 foams [8].

Ultra-macro-porosity (>100 μm) was investigated by image analysis (Image Pro Plus 6.0., Media Cybernetics, Inc. Bethesda, MD, USA) of high resolution photos (scanner Sharp JX330, Japan) and of scanning electron micrographs of the cross sections.

Pore size distribution in the range 0.0058–100 μm was analyzed by mercury porosimetry (Thermo Finnigan Pascal 140 and Thermo Finnigan Pascal 240). Measurements of specific surface area, pore volume and pore size distributions in the 1000–2 nm range were carried out in a Micromeritics ASAP 2020 instrument by N_2 adsorption/desorption at −196 °C. Samples were previously degassed under vacuum, heated up to 250 °C and maintained for 60 min at a pressure below 30 μmHg. Specific surface area was calculated by the Brunauer–Emmet–Teller (BET) method. The total pore volume was obtained at $p/p^0 = 0.995$. Pore size distributions were obtained by the BJH method using the desorption branch. The analyses were made on blended powders belonging to at least three grounds and 600 μm sieved samples of the same compositions. The error in the measures is related to the accuracy of Hg intrusion porosimetry (4%) and N_2 adsorption/desorption technique (1%).

The degree of sample polymerization, i.e. the transformation of metakaolin to geopolymers was monitored by ^{27}Al MAS NMR spectroscopy. ^{27}Al MAS NMR single pulse spectra were recorded using a Bruker Avance 500 MHz (11.7 T) Wide Bore spectrometer with 4 mm o.d. ZrO_2 rotors with a rotation speed of 12 kHz and high-power decoupling pulse sequences with π/12 (0.7 μs) excitation pulse. The ^{27}Al NMR observed chemical shift was referred to an aqueous solution of $Al(NO_3)_3$. Spectra of geopolymer samples and parent metakaolin were simulated using Dmfit software.

The accessibility of the inner volume of geopolymers was determined employing the ion exchange capacity of geopolymer for NH_4^+ ions. The replacement of Na^+ and K^+ ions in geopolymers by NH_4^+ ions during ion exchange was reported [9,19]. Ion exchange capacity of geopolymer for small cations (Co^{2+} and NH_4^+) was suggested as a measure of geopolymerization degree of geopolymer and accessibility of the inner volume of geopolymer network [9]. The maximum NH_4^+ exchanged form of geopolymers was obtained by repeated equilibration of the sample with a 0.5 M aqueous solution of NH_4NO_3 at RT (100 ml of solution per 1 g of geopolymer applied thrice over 36 h). After the ion exchange procedure, the geopolymers were carefully washed with distilled water to remove all the excess NH_4^+ ions. The obtained NH_4-geopolymers were dried at room temperature in the open air to receive fully hydrated NH_4-geopolymers. The concentration of NH_4^+ ions in the sample was determined by the FTIR spectroscopy of N–H vibration.

The FTIR spectra were recorded on a NICOLET 6700 spectrometer using a DTGS KBr detector following the procedure described elsewhere [19]. For a single spectrum, 128 scans at

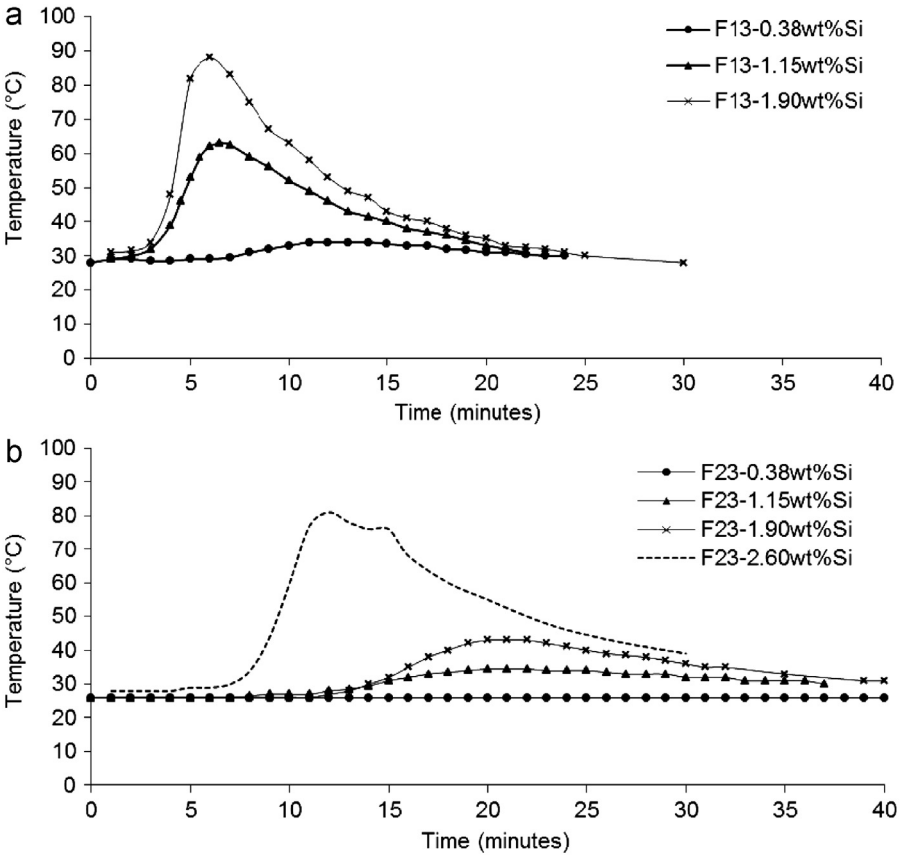

Fig. 2. Plots of temperature vs. time registered at RT in geopolymer slurries upon metallic Si addition: F13 (a) and F23 (b) geopolymeric based foams.

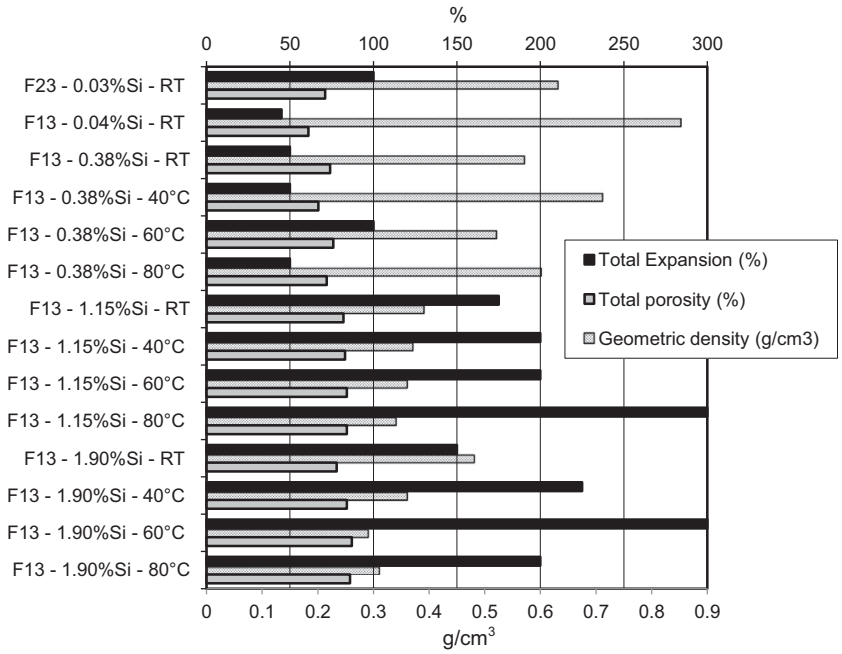

Fig. 3. Foam expansion, bulk density and total porosity of F13 and F23 foams.

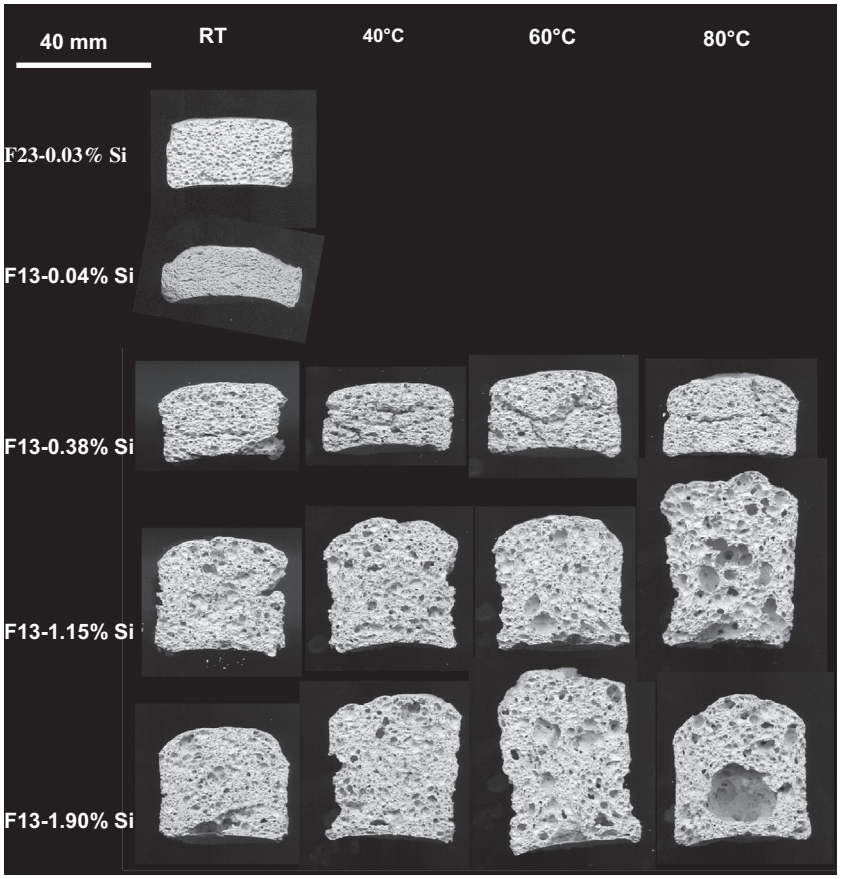

Fig. 4. High resolution photos of the cross section of F13 and F23 foams obtained with different metallic silicon additions and curing temperatures.

$2\ cm^{-1}$ resolution were collected. The samples were prepared in the form of thin self-supporting pellets with a thickness of about $10\ mg\ cm^{-2}$ mounted in a sample holder and directly measured in the open air. Quantitative analysis of the intensity of the IR band of N–H deformation vibration of NH_4^+ ions yields the concentration of NH_4^+ ions. Spectra intensities were normalized on the standard

sample thickness of 10 mg cm^{-2}, the extinction coefficient for the IR band of the N–H vibration at 1445 cm^{-1} was $\varepsilon_{NH} = 13.0 \pm 0.6$ cm μmol^{-1}.

3. Results

3.1. Slurries characterization

Before metallic silicon addition, the starting geopolymer slurries exhibited a plastic behavior. The logarithmic plots of viscosity vs. shear rate (Fig. 1a and b) followed a power law with exponent close to −1 [20] for both the compositions. The viscosity was greatly dependent on the molar ratio H_2O/K_2O, being the viscosity of slurry with $H_2O/K_2O = 13.5$ five order of magnitude higher than that of the slurry with $H_2O/K_2O = 23.0$.

The addition of the metal silicon to the geopolymer slurries produces the exothermic reaction (1), with consequent increase of temperature related to the amount of silicon added. The temperature increase in the various mixtures as a function of the added silicon is reported in Fig.2a and b. The higher the

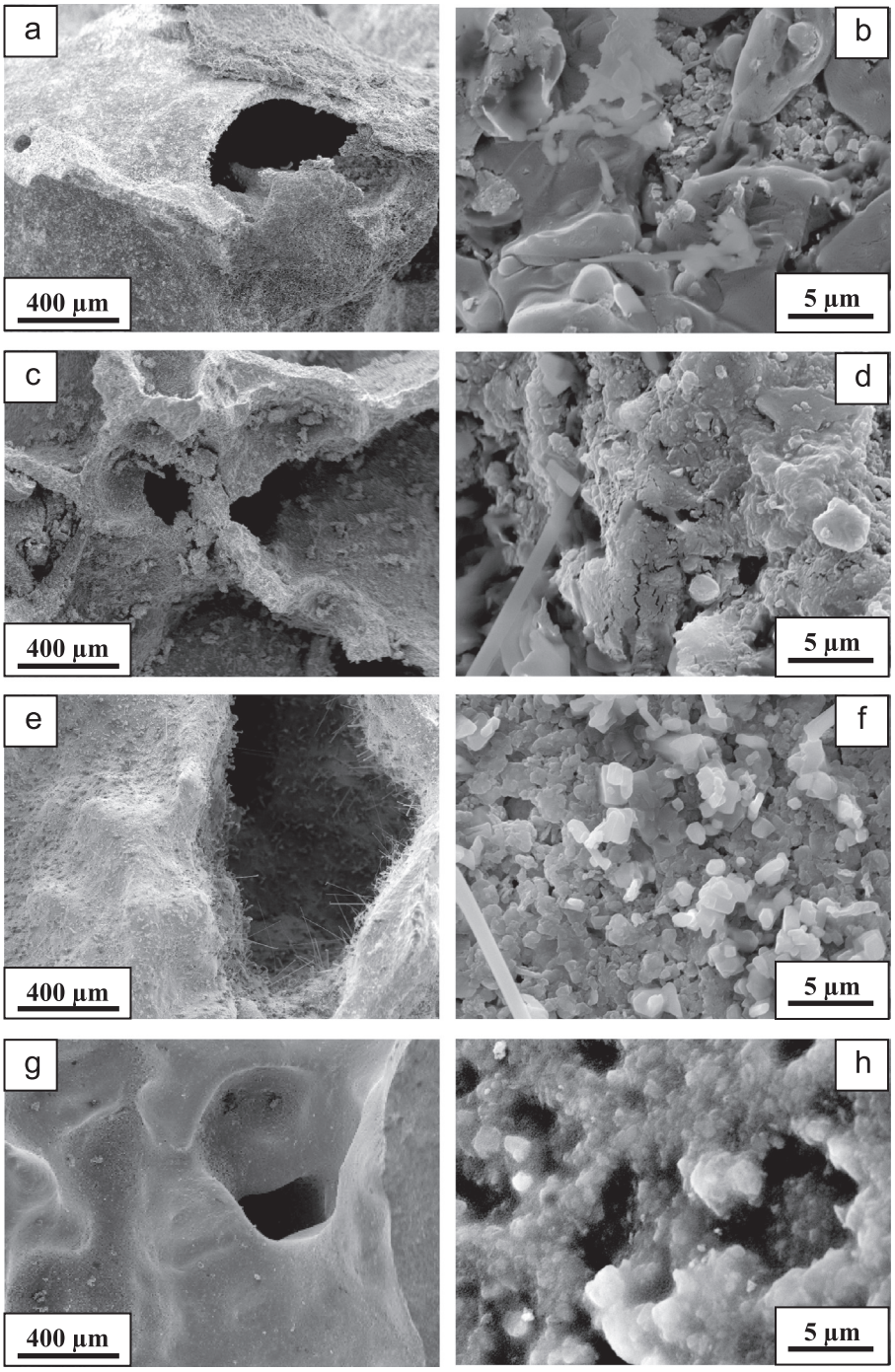

Fig. 5. SEM micrographs of F13-1.15%Si-80 °C (a, b), F13-1.15%Si-RT (c, d), F13-0.38%Si-RT (e, f) and F13-0.04%Si-RT (g, h).

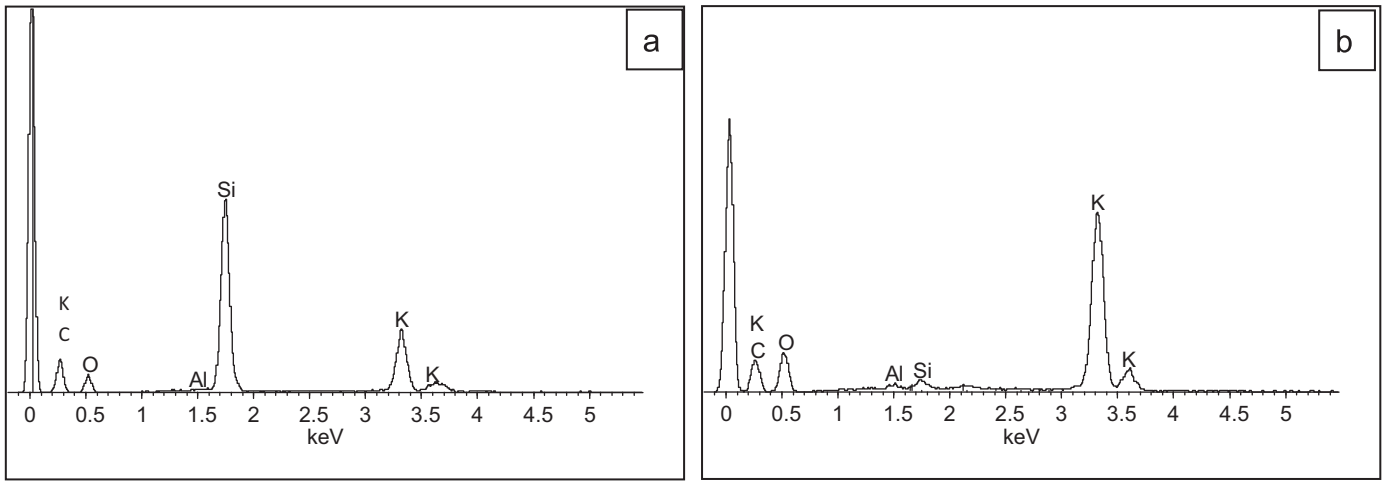

Fig. 6. EDS analyses on residual potassium silicate in F13-1.15%Si-80 °C (a) and needles formed on the surface of F13-0.38%Si-RT (b).

water dilution (such as in foams F23) the lower the temperature increase and longer the time to warm the suspension.

3.2. Foams formation and macro- and micro-structures

Foams expansion, as well as geometric density and total porosity values are reported in Fig. 3. The above properties were all dependent on Si^0 amount, curing temperature and H_2O/K_2O (=13.5 and 23.0) molar ratios, i.e. water amount of the slurry. Si additions of 2.60 wt% gave rise to destroyed architectures and thus the corresponding samples are not included in Fig. 3.

High resolution photos after expansion and curing of the geopolymer foams F13 and F23 are reported in Fig. 4. Ultra-macro-pores are observable in all samples.

Foams F13 showed a nonuniform distribution of the ultra-macro pores in terms of dimension and shape; in particular some prolate pores with an aspect ratio ranging from 2 to 5 were aligned perpendicularly to the expansion direction. As expected, foams expansion increased with curing temperature (Figs. 3 and 4). A quite low quantity of silicon (sample F13-0.38%Si) led to little expanded structures. Ultra-macro-pores ranged from 250 μm to 3 mm, while the center of the samples showed cracks, attributable to thermal stresses occurring during water evaporation. In the samples F13-1.15%Si and F13-1.90%Si, the expansion increased, with ultra-macro-pores in the range between 250 μm and 8 mm. In F13-1.15%Si-80 °C and F13-1.90% Si-80 °C coalescence of gas bubble occurred leading to internal voids up to 20 mm.

Foams F23 with Si addition higher than ~0.3 wt% collapsed in relation to the higher water content of the starting mixture with respect to that of the samples F13. Conversely, F23-0.03% Si-RT (Figs. 3 and 4) had a regular distribution of rounded ultra-macro-pores that ranged from 200 μm to 1 mm in diameter [8].

SEM micrographs of the surfaces of pore walls of the F13 foams are shown in Fig. 5. The surface of all samples was very different from the typical microstructure of an un-foamed mesoporous geopolymer matrix mainly formed by nano-precipitates

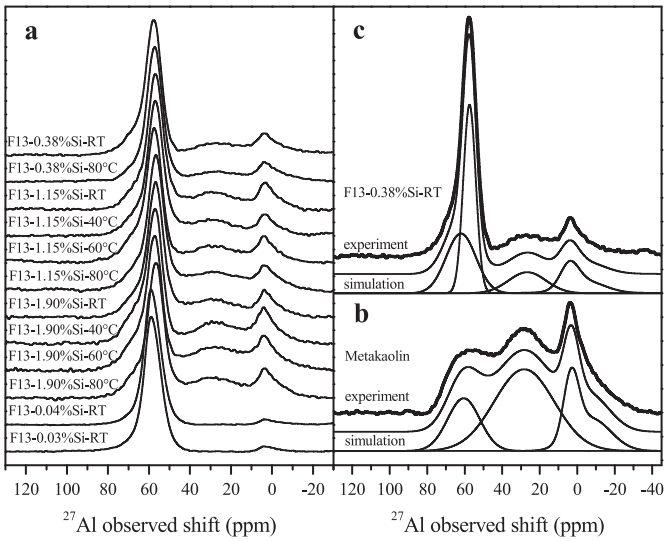

Fig. 7. ^{27}Al MAS NMR single pulse spectra of geopolymer foams (a), ^{27}Al MAS NMR single pulse spectrum of parent metakaolin and its simulation (b), and ^{27}Al MAS NMR single pulse spectrum of sample F13-0.38%Si-RT and its simulation (c).

[5,7,8]. In particular particles packing, surface cracking, enrichment in potassium silicate and needle like phases were observed.

Potassium silicate was present on the surface when both Si amount and curing temperature were increased (sample F13-1.15% Si-80 °C, Fig. 5b and EDS spectrum in Fig. 6a). Filaments based of potassium carbonates were detected when curing was at RT (F13-1.15%Si-RT and F13-0.38%Si-RT in Fig. 5d and f and EDS spectrum in Fig. 6b).

3.3. Polymerization degree and accessibility of geopolymer inner volume

^{27}Al MAS NMR spectra of foamed samples and of metakaolin are depicted in Fig. 7.

^{27}Al resonance around 60 ppm reflecting tetrahedral Al atoms prevails only in ^{27}Al MAS NMR single pulse spectrum of samples F13-0.04%Si-RT and F23-0.03%Si-RT. The ^{27}Al MAS

Table 2
Total porosity and average pore diameter measure by Hg intrusion and specific surface areas calculated through the BET (S_{BET}) method and pore volume (V_p) values of F13 and F23 foams. The error is ±4% and ±1%, respectively for Hg intrusion porosimetry and N_2 adsorption–desorption measures.

Sample	Hg intrusion		S_{BET} (m^2/g)	V_p (cm^3/g)
	Total porosity (%)	Average pore diameter (μm)		
F13-1.15%Si-RT	34	98	1	0.005
F13-1.15%Si-80 °C	32	96	1	0.005
F13-0.04%Si-RT	37	0.03	50	0.240
F23-0.03%Si-RT	34	0.03	98	0.480

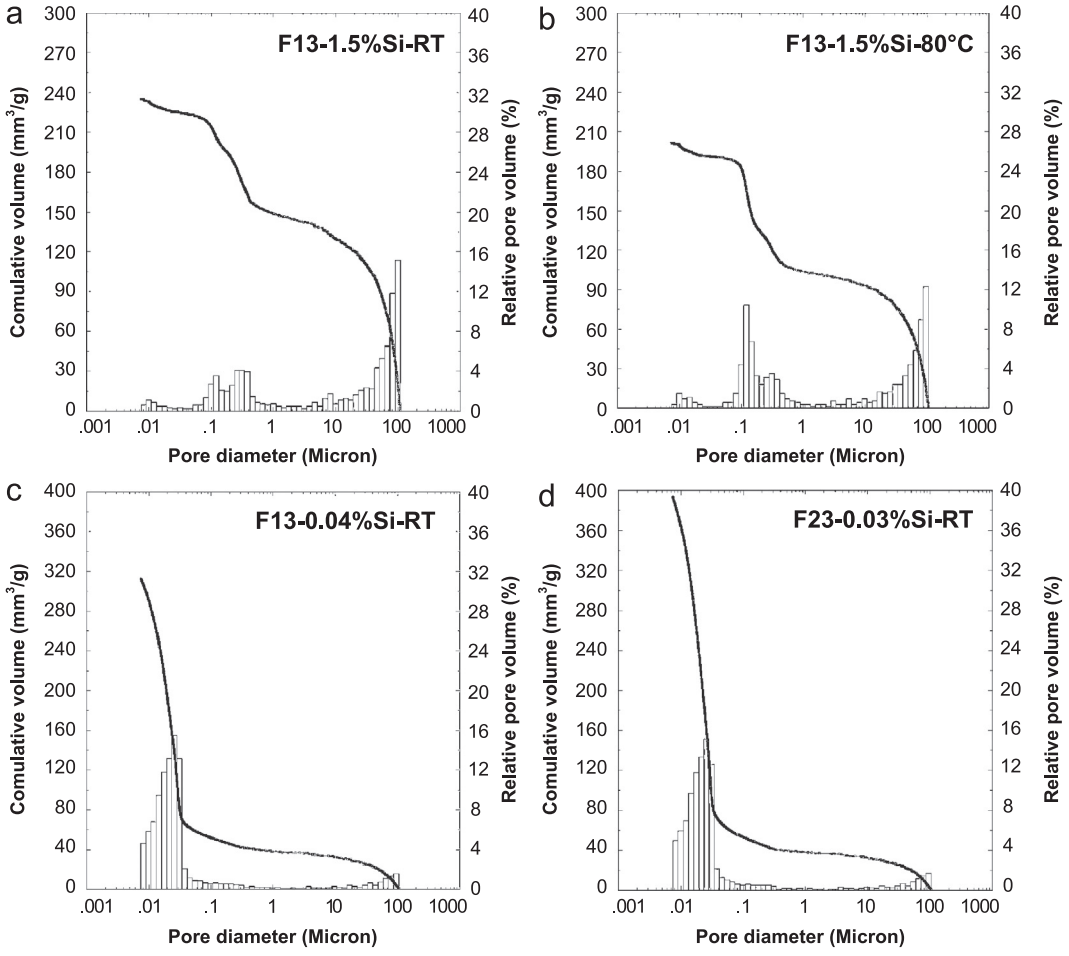

Fig. 8. Pore size distribution by Hg intrusion of F13-1.15%Si-RT (a), F13-1.15%Si-80 °C (b), F13-0.04%Si (c) and F23-0.03%Si (d).

NMR spectra of all other geopolymer foams exhibit significant intensity of resonances around 0 and 30 ppm reflecting octahedral and penta-coordinated Al, see Fig. 7a. As Al atoms in geopolymer network exhibit exclusively tetrahedral coordination, the presence of octahedral and penta-coordinated Al atoms clearly evidence the presence of residual un-reacted metakaolin in samples and thus, their only partial polymerization. ^{27}Al MAS NMR spectrum of parent metakaolin MK1200S and its simulation is given in Fig. 7b. According to the spectrum simulation, asymmetric resonance with maximum at 3 ppm corresponds to octahedral, resonance centered around 27 ppm to penta-coordinated and resonance with maximum between 60 and 65 ppm to tetrahedral Al of metakaolin. Simulation of the ^{27}Al MAS NMR spectra of geopolymer samples (an example is illustrated in Fig. 7c) evidence beside resonances corresponding to Al atoms of metakaolin the presence of new resonance with maximum between 55 and 58 ppm reflecting tetrahedral Al atoms of geopolymer network and dominating spectra of all samples. The presence of resonance around 60 ppm of tetrahedral Al of residual metakaolin is reflected in the shoulder of

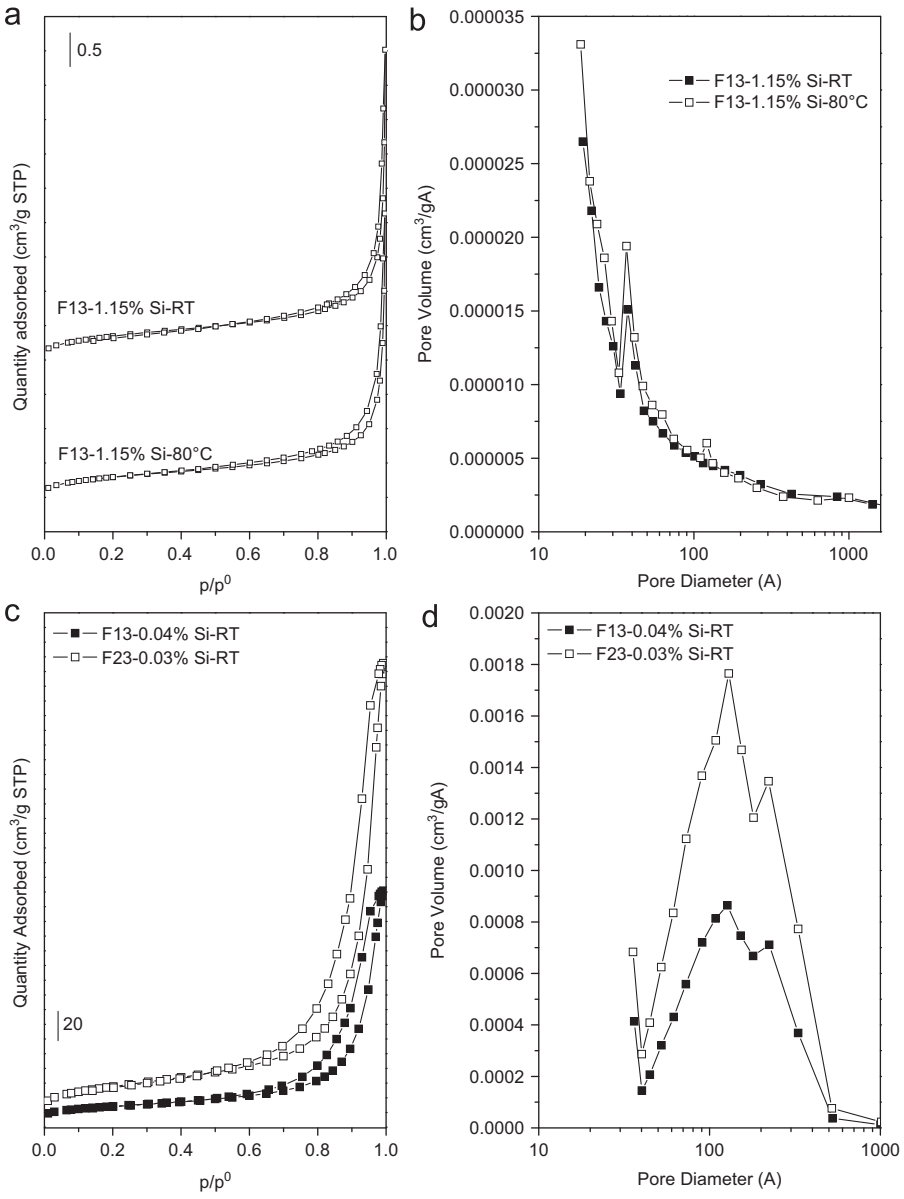

Fig. 9. N_2 adsorption/desorption isotherms at −196 °C (a, c) and BJH pore size distributions (b, d) of of F13-1.15%Si-RT and F13-1.15%Si-80 °C (a, b), F13-0.04%Si and F23-0.03%Si (c, d).

the band of tetrahedral Al. The value of ^{27}Al observed chemical shift of tetrahedral Al in the geopolymer network is in agreement with values reported earlier, see e.g. Refs. [10,18]. Thus, simulations of the ^{27}Al MAS NMR spectra allows us to estimate polymerization degree of investigated geopolymer foams using the following equation:

$$\text{Polymerization degree} = I_G/I_{TOTAL} \quad (3)$$

where I_G is the intensity of the signal of tetrahedral Al in geopolymer at 55–58 ppm and I_{TOTAL} is the total intensity of the ^{27}Al NMR single pulse spectrum. The polymerization degree of geopolymer foams according to Eq. (3) ranges 30–97% and is reported in Table 1.

A large amount of silicon influences negatively the polymerization which ranges 30–56% with the exception of samples F13-0.04%Si-RT and F23 0.03%Si-RT that are effectively geopolymers. In F13-1.15%Si, the maximum of polymerization was observed with curing at 60 °C, while in F13-1.90%Si with curing at 40 °C.

It should be noted that the low degree of NH_4^+ exchange capacity (ca. 25%, Table 1) of F13-0.04%Si-RT and F23-0.03% Si-RT samples, which are almost completely polymerized (97%).

3.4. Porosimetric and specific surface characterizations

In F13-1.15%Si (RT and 80 °C) foams the average pore diameters measured by Hg intrusion were similar (Table 2).

Both samples presented bimodal pore size distributions (Fig. 8a and b): the relative pore volume percentage in the ranges 0.1–1 μm and 10–100 μm were respectively ~40% and ~60% for F13-1.15%Si-RT, 50% and 50% for F13-1.15%Si-80 °C. The samples with a smaller quantity of silicon, F13-0.04%Si-RT and F23-0.03%Si-RT, had pores mainly ranging between 0.01 and 0.1 μm (Fig. 8c and d) with dimensions comparable to those of un-foamed matrices [8].

N_2 adsorption/desorption measurements were performed on ground foams to obtain information about the pores that are out of the detection range of Hg porosimetry. The results are reported in Table 2 and Fig. 9. It was evidenced that the measured specific surface areas decreased by increasing the silicon content in the starting mixtures.

The samples F13-1.15%Si-RT and F13-1.15%Si-80 °C have very similar textural properties, with rather low values of the BET surface area and total pore volume (Table 2). Both isotherms (Fig. 9a and b) belong to Type II from the IUPAC classification [21], and are characteristic of non-porous or macro-porous materials. The isotherms are almost superimposable, with a very narrow hysteresis loop. The differential distribution of the pore dimensions, calculated by the BJH method, confirms the absence of meso-pores, as the peak at about 36 Å can be considered as an artifact of the method itself.

The isotherms of F13-0.04%Si-RT and F23-0.03%Si-RT are very similar in form and are of Type IV with H_2 hysteresis (Fig. 9c and d). BJH pore size distributions show two maxima at about 130 and 220 Å, the amount of the smaller pores being larger.

4. Discussion

4.1. Effect of metallic silicon addition on foaming and macrostructure

Foams formation and the related macro- and micro-structures are influenced both by rheological (viscosity) and thermal parameters. Volume expansion, macropores dimension and prolate shape belong to the balance of the thermodynamics of reaction (1), viscosity and geopolymerization or hardening.

Foam expansion and increase of pore dimension are favoured by increasing the addition of Si and the curing temperature as shown in Figs. 3 and 4. The developed ultramacro porosity ranging from a few hundreds of microns to a few tenths of millimeters are consistent with the data previously obtained by inorganic in situ foaming of SiC based foams, where the foaming agent was the metallic Si impurities in the raw powders [15,16], and with results reported by other authors [14,22].

Obviously the use of higher quantity of silicon produces more H_2 gas, while the increase in curing temperature induces higher and faster formation of hydrogen bubbles; in fact reaction (1) is favoured by temperature increase as all gas forming reaction, considering that ΔG^0 changes from −359.4 kJ/mol at 25 °C to −366.6 kJ/mol at 80 °C [15]). From this point of view the viscosity of the starting slurries plays an important role in foam formation.

This general trend faces with the viscosity of the starting slurries (Fig. 1) and the thermal effects related to reaction (1) (Fig. 2).

The low viscosity of the F23 slurry (Fig. 1b) allows to obtain well foamed materials only if very low amounts of silicon is added, since the hydrogen spreads easily through the reaction mixture. Furthermore, low viscosity facilitates the coalescence of bubbles of hydrogen, which lead to the collapse of the structure when the gas pressure exceeds the surface tension in the pore. In the case of the more viscous F13 slurries, the contemporary use of 80 °C as curing temperature and high amount of Si as in samples F13-1.15%Si-80 °C and F13-1.90%Si-80 °C lead to coalescence of voids up to 20 mm (Fig. 4) because of enhanced gas evolution but also of fast consolidation. The warming of the slurries (Fig. 2) by increasing Si^0 addition decreases the time of consolidation due to the reduction of available water. In detail, water evaporation is favored by temperature increase and consequently hardening occurred. Moreover, consumption of water is proportional to metallic silicon addition because of the reduction of water concerning di-hydrogen formation [15]

$$4H_2O + 4e^- \rightarrow 2H_2 + 4OH^- \quad (4)$$

The exothermal reaction (1) affects also microstructure and properties directly acting on the degree of polymerization as explained in Section 4.2.

4.2. Effect of metallic silicon addition on polymerization degree and correlation with microstructure

Metallic Si addition affects the polymerization degree and consequently the final microstructure and meso-porosities by favouring water removal from the reacting slurries and fast consolidation because of the exothermic and water consuming reaction (1).

In closed systems, geopolymerization is generally favored by the increase in temperature, as setting time is faster at high temperature [23] because it is favored in hydrothermal conditions [24]. Moreover, water is the reaction medium during geopolymerization.

The geopolymerization mechanism is quite complex [5], but may be simplified into a few steps [25]: water-consuming dissolution of the aluminosilicate powder by alkaline hydrolysis, condensation, gelation, reorganization, polymerization and hardening. When the main reaction changes from hydrolysis (consuming water) to polycondensation (releasing water), too much water can hinder the polycondensation kinetically [26], since water is a product of the reaction itself, and setting stage should be prolonged. Since water entrance into the geopolymer framework is limited, it gives rise to a steric hindrance and acts as a pore-forming agent upon its removal during setting at 80 °C [26–28].

The morphologies and compositions of external surfaces of F13 foamed samples (Fig. 5) are caused by surface tension and faster consolidation of the surface than of the bulk. This two phenomena cause particles packing, surface cracking, enrichment in potassium silicate and needle like phase formation.

As stated before, the redox reaction (1) removes water from the system to form hydrogen (reduction reaction of water). Contemporary water evaporation occurs due to the rising of temperature, consequent to this exothermic reaction. By moving the reaction medium (water) quickly away, metakaolin lamellae reacts only superficially and unreacted potassium silicate covers them, thus preventing any further metakaolin dissolution. Potassium silicate was observed on the surface of samples cured at 80 °C (sample F13-1.15%Si-80 °C, Fig. 5b). The EDS analysis (Fig. 6a) detected an atomic ratio Si/K slightly higher than the nominal one of the starting potassium silicate aqueous solution. This is probably due to the partial incorporation of reacted metallic silicon in the form of $Si(OH)_4$. However a reliable exact evaluation of the phase composition in terms of atomic ratio was however impossible due to the intrinsic limits of the analysis.

In the F13-0.38%Si foams the increase of temperature (Fig. 2a) and water subtractions by reaction (1) are quite modest. The formation of needles based of potassium carbonates (Fig. 6b) could be attributed to carbonate impurities in KOH and to absorbed CO_2 in starting SiO_2 or to atmospheric CO_2 reacting with the alkali system [29].

In foams F13-0.04%Si-RT, apart for a surface particle packing due to surface tension caused by gas evolution, no presence of alkali rich phases were detected, as well in foam F23-0.03%Si-RT [8]. The final microstructure of a fully reacted geopolymer consists of nano-particles separated by nano-pores. Vice versa, with high amounts of silicon added to produce foams, this characteristic disappears, then the reaction of geopolymerization is influenced by the exothermic reaction of silicon in the alkali aqueous solution, which hinders its completion. A kinetic balance between geopolymerization and redox reaction is needed to produce fully reacted foams.

The porosimetric and specific surface area data (Table 2) are in agreement with those of MAS-NMR analysis indicating the polymerization degree and reflecting in ion exchange capacity (Table 1), since F13-0.04%Si-RT and F23-0.03%Si-RT with 97% of polymerization degree shows the higher specific surface areas and the smaller pore dimension.

Since porosimetric analyses by Hg intrusion were performed on ground and 600 μm sieved foams, the results were representative of the porosity of the ultramacro-pore walls, i.e. the porosity of the geopolymer matrices formed at the process condition. Pores below 10 μm belong to the geopolymer intrinsic porosity and water steric effect, while pores ranging from 10 to 100 μm are due to the foaming process [8]. As already discussed, the relative pore volume percentage in the ranges 0.1–1 μm and 10–100 μm were respectively ~40% and ~60% for F13-1.15%Si-RT, 50% and 50% for F13-1.15%Si-80 °C (Table 2). The samples with a smaller quantity of silicon, F13-0.04%Si-RT and F23-0.03%Si-RT, had pores mainly ranging between 0.01 and 0.1 μm (Fig. 8c and d) with dimensions comparable to those of un-foamed matrices [8].

Concerning N_2 adsorption/desorption measurements, in analogy with zeolites, the fact that significant fraction of the geopolymer inner volume is accessible through 8-member or smaller rings can affect surface area measurement using N_2. K^+ cations upon dehydration preferentially occupy cationic sites formed by 8-member rings [30,31] and block N_2 transport through these rings [23,32]. Thus, although significant part of inner volume of geopolymer particulates might be accessed by solvated cations which migrate through eight rings [9], the surface area of geopolymer measured using N_2 adsorption represents predominantly surface of meso-pores, i.e. outer surface of nanosized particulates forming geopolymer, as was already suggested [19].

Low values of specific surface area of samples F13-1.15%Si-RT and F13-1.15%Si-80 °C can be attributed to the presence of unreacted potassium silicate which surrounds the precipitates and particles of non-reacted metakaolin, filling the meso-pores and determining a decrease of the surface area in partially polymerized samples.

As previously observed [8], after the foaming process with very small metallic silicon addition S_{BET} values increased in respect with reference "unfoamed" geopolymer matrix, namely from 40 to 50 $m^2\ g^{-1}$ for the sample prepared with a molar ratio $H_2O:K_2O = 13.5$ and from 16 to 98 $m^2\ g^{-1}$ when $H_2O:K_2O = 23.0$ was used. It should be pointed out that monolith with the hierarchic pore system, meso-pore surface area ranging 100 $m^2\ g^{-1}$ and high Al content enabling accommodation of a high concentration of metal ion species with properties similar as those in zeolites [19] exhibits a high potential for catalytic applications.

Finally it should be noted the low degree of NH_4^+ exchange capacity which is in the range 11–27% for all samples (Table 1). The low degree of NH_4^+ exchange capacity (ca. 25%) (Table 1) of almost completely polymerized samples (F13-0.04%Si-RT and F23-0.03%Si-RT with 97% of polymerization degree) indicates that only one quarter of the geopolymer inner volume is accessible for solvated cations sizing the potassium one through regular 8-member or larger rings, through which solvated K^+ ions can migrate. The smallest ring (with 3.7 Å diameter) enabling full ion exchange of K^+ ions was reported for chabazite [33]. The rest of K^+ ions, and thus, network Al atoms, are located in channels/cavities accessible only through significantly deformed 8 rings or smaller rings. This indicates that the outer one quarter of nano-particulates ranging from 5 to 15 nm [6] forming geopolymer volume will be accessible for incorporation of smaller cations as e.g. Co^{2+}, Cu^{2+}, Fe^{2+} or Fe^{3+}, which will be accessible through 8-member or larger rings and can play a role of catalytic centers similarly as in zeolites [19]. This limited accessibility concerns also geopolymer fraction of the foams with lower polymerization degree. Also in these samples the accessible part of geopolymer represents from one-third to one-half of geopolymer inner space. In addition, it should be pointed out that the accessibility of the inner volume of geopolymer network was reduced consequently to low polymerization degrees.

5. Conclusions

Addition of metallic Si allows to obtain geopolymer foams thanks to its redox reaction in an alkaline environment causing evolution of H_2 gas. However, the silicon addition must be controlled to limit the water depletion in the geopolymer matrix. High silicon content

adversely affects the reaction of geopolymerization, in particular when associated with high temperatures of consolidation (80 °C). In fact, the Si redox reaction consumes water of the geopolymer matrix system, thus reducing the amount availablility for geopolymerization. In addition, a high curing temperature and the exothermicity of the Si reaction causes a fast evaporation of water, which reflects in further decrease of the available reaction medium. High contents of silicon determine a low geopolymerization degree, as evidenced by ^{27}Al MAS-NMR analysis.

A low degree of geopolymerization decreases the accessibility of the matrix determined by ion exchange and the intrinsic meso-porosity determined by desorption of N_2.

Acknowledgment

The financial supports by the Italian Ministry of University and Research and the National Research Council of Italy are gratefully acknowledged.

E.P.: The Authors thank the foundation "Toso Montanari" for the grant obtained.

References

[1] K. Okada, T. Isobe, K. Katsumata, Y. Kameshima, A. Nakajima, K.J. D. MacKenzie, Porous ceramics mimicking nature—preparation and properties of microstructures with unidirectionally oriented pores, Science and Technology of Advanced Materials 12 (064701) (2011) 11.

[2] T. Tomita, S. Kawasaki, K.J. Okada, A novel preparation method for foamed silica ceramics by sol–gel reaction and mechanical foaming, Porous Materials 11 (2004) 107–115.

[3] V. Medri, M. Mazzocchi, A. Bellosi, ZrB_2-based sponges and lightweight devices, International Journal of Applied Ceramic in Technology 8 (2011) 815–823.

[4] P. Colombo, Conventional and novel processing methods for cellular ceramics, Philosophical Transactions of the Royal Society A 364 (2006) 109–124.

[5] J. Davidovits, Geopolymers Chemistry and Applications, Institut Geopolymere, Saint-Quentin, France, 2008.

[6] M. Gordon, J. Bell, W.M. Kriven, Geopolymers: alkali bonded ceramics (ABCs) for high-tech applications, Ceramic Transactions 175 (2006) 215–224.

[7] W.M. Kriven, J.L. Bell, M. Gordon, Microstructure and microchemistry of fully-reacted geopolymers and geopolymer matrix composites, Ceramic Transactions 153 (2003) 227–250.

[8] E. Landi, V. Medri, E. Papa, J. Dedecek, P. Klein, P. Benito, A. Vaccari, Alkali-bonded ceramics with hierarchical tailored porosity, Applied Clay Science 73 (2013) 56–64.

[9] O. Bortnovsky, J. Dedecek, Z. Tvaruzkova, Z. Sobalik, J. Subrt, Metal ions as probes for characterization of geopolymer materials, Journal of the American Ceramic Society 91 (2008) 3052–3057.

[10] V. Medri, S. Fabbri, J. Dedecek, Z. Sobalik, Z. Tvaruzkova, A. Vaccari, Role of the morphology and the dehydroxylation of metakaolins on geopolymerization, Applied Clay Science 50 (2010) 538–545.

[11] R. Studart, U.T. Gonzenbach, E. Tervoort, L.J. Gauckler, Processing routes to macroporous ceramics: a review, Journal of the American Ceramic Society 89 (2006) 89–1771.

[12] W. Van Bonin, U. Nehen, Hydrogen Peroxides Blowing Agent for Silicate Foams, US Patent 3,864,137, 1975.

[13] J.L. Bell, W.M. Kriven, Preparation of ceramic foams from metakaolin-based geopolymer gels, in: H.T. Lin, K. Koumoto, W.M. Kriven, E. Garcia, I.E. Reimanis, D.P. Norton (Eds.), Developments in Strategic Materials: Ceramic Engineering and Science Proceedings, vol. 29 (10), 2009, pp. 97–111.

[14] E. Prud'homme, P. Michaud, E. Joussein, C. Peyratout, A. Smith, S. Rossignol, In situ inorganic foams prepared from various clays at low temperature, Applied Clay Science 51 (2011) 15–22.

[15] V. Medri, A. Ruffini, Alkali-bonded SiC based foams, Journal of the European Ceramic Society 32 (2011) 1907–1913.

[16] V. Medri, A. Ruffini, The influence of process parameters on *in situ* inorganic foaming of alkali-bonded SiC based foams, Ceramic International 38 (2011) 3351–3359.

[17] X.G. Zhang, Electrochemistry of Silicon and its Oxide, Kluver Academic/Plenum Publishers, New York, 2001.

[18] V. Medri, S. Fabbri, A. Ruffini, J. Dedecek, A. Vaccari, SiC-based refractory paints prepared with alkali aluminosilicate binders, Journal of the European Ceramic Society 31 (2011) 2155–2165.

[19] P. Sazama, O. Bortnovsky, J. Dedecek, Z. Tvaruzkova, Z. Sobalik, Geopolymer based catalysts—new group of catalytic materials, Catalysis Today 164 (2011) 92–99.

[20] D.C.-H. Cheng, Yield stress: a time-dependent property and how to measure it, Rheologica Acta 25 (1986) 542–554.

[21] K.S.W. Sing, D.H. Everett, R.A.W. Haul, L. Moscou, R.A. Pierotti, J. Rouquerol, Reporting physisorption data for gas/solid systems with special reference to the determination of surface area and porosity, Pure and Applied Chemistry 57 (1985) 603–619.

[22] W.D.A. Rickard, L. Vickers, A. van Riessen, Performance of fibre reinforced, low density metakaolin geopolymers under simulated fire conditions, Applied Clay Science 73 (2013) 71–77.

[23] A. Polesquen, F. Frizon, D. Lambertin, Rheological behaviour of alkali-activated metakaolin during geopolymerization, Journal of Non-Crystalline Solids 357 (2011) 3565–3571.

[24] J.L. Provis, G.C. Lukey, J.S.J. van Deventer, Do geopolymers actually contain nanocrystalline zeolites? A reexamination of existing results, Chemistry of Materials 17 (2005) 3075–3085.

[25] P. Duxon, A. Fernandez-Jimenez, J.L. Provis, G.C. Luckey, A. Palomo, J.S.J. Van Deventer, Spectroscopic studies of alkaline activated slag geopolymers, Journal of Materials Science 42 (2007) 2917–2933.

[26] Z. Zuhua, Y. Xiao, Z. Huajun, C. Yue, Role of water in the synthesis of calcined kaolin-based geopolymer, Applied Clay Science 43 (2009) 218–223.

[27] K. Okada, A. Ooyama, T. Isobe, Y. Kameshima, A. Nakajima, K.J. D. MacKenzie, Water retention properties of porous geopolymers for use in cooling applications, Journal of the European Ceramic Society 29 (2009) 917–923.

[28] F. Frizon, C. Joussot Dubien, Method of Preparing a Controlled Porosity Geopolymer, The Resulting Geopolymer and the Various Applications Thereof, Patent Publication no. US2010 0222204 A1, 2010.

[29] S.T. Hyde, A.M. Carnerup, A.K. Larsson, A.G. Christy, J.M. Garcia-Ruiz, Self assembly of carbonate silica colloids: between living and non-living form, Physica A 339 (2004) 24–33.

[30] J.J. Pluth, J.V. Smith, Crystal-structure of dehydrated potassium-exchanged zeolite A. Absence of supposed zero-coordinated potassium—refinement of Si, Al-ordered superstructure, Journal of Physical Chemistry 83 (1979) 741–749.

[31] B. Civalleri, A.M. Ferrari, M. Llunell, R. Orlando, M. Merawa, P. Ugliengo, Cation selectivity in alkali-exchanged chabazite: an ab initio periodic study, Chemistry of Materials 15 (2003) 3996–4004.

[32] F.N. Ridha, Y.X. Yang, P.A. Webley, Adsorption characteristics of a fully exchanged potassium chabazite zeolite prepared from decomposition of zeolite Y, Microporous and Mesoporous Materials 117 (2009) 497–507.

[33] J. Shang, G. Li, R. Singh, P. Xiao, J.Z. Liu, P.A. Webley, Potassium chabazite: a potential nanocontainer for gas encapsulation, Journal of Physical Chemistry C 114 (2010) 22025–22031.